Arch. Metall. Mater. **68** (2023), 2, 639-648

DOI: https://doi.org/10.24425/amm.2023.142445

A.S. CHAUS[1*], Ľ. ČAPLOVIČ[1], A.I. POKROVSKII[2], R. SOBOTA[1]

MICROSTRUCTURE AND PROPERTIES EVALUATION OF DUCTILE CAST IRON SUBJECTED TO HOT PLASTIC DEFORMATION AND AMBIENT TEMPERATURE COMPRESSION

The as-cast microstructure of ductile cast iron (DI) was investigated using light microscopy (LM) and SEM techniques. Further the influence of hot plastic extrusion at 1000°C with plastic strain in the range of 20-60-80% on the transformation of the as-cast microstructure and on the mechanical properties was studied. Besides this, the microstructure of DI subjected to hot extrusion after the fracture of the corresponding samples induced by compression tests was thoroughly investigated. It was found that compression had a dramatic influence on a shear deformation and hence shear fracture of the compressed samples. It was shown that the shear fracture of the hot deformed ductile iron is accompanied by the occurrence of a narrow zone of severe plastic deformation. The fracture surfaces of the extruded samples subjected to the tensile tests and the compression tests were examined.

Keywords: Ductile iron; Plastic deformation; Microstructure; Properties; Fracture surfaces

1. Introduction

Different types of cast irons due to their excellent castability and low cost are widely used in many engineering applications [1,2]. Ductile (nodular) cast iron with spheroidal (nodular) graphite (further DI), compared with other cast irons, has the best combination of mechanical properties, which makes this iron currently the most prospect foundry alloy [3-7]. The latter is primarily attributed to the favourable shape of graphite developed in the as-cast microstructure during solidification. This favourable graphite shape is achieved by a special treatment of a melt prior casting, i.e., by adding spheroidasing elements to the melt, most commonly magnesium. In this context it is worth mentioning that since the introduction of DI a lot of theories has been suggested to explain the mechanism of different graphite shape formation under varying conditions [8-16]. However, there is no theory currently available to explain the formation of graphite spheroid comprehensively, moreover, often some of these theories are controverse, as can be seen, for example, when reading the resent papers published in the very reputable journals [8,11]. Primarily, this can be referred to the origin of nuclei sites for graphite spheroids. For example, the complex origin of nuclei in DI in relation to their chemistry, i.e., concerning such elements as Mg, S, O, Si, and other, has been reported in many papers [8-10,17-21].

On the other hand, the tensile and fatigue strength of DI is considered as a drawback which does not allow DI to compete with forged steels [22]. However, our previous works showed that the cold plastic deformation [23] and especially the hot plastic deformation [24,25] could improve the tensile strength of this material. From the practical application point of view, it could be important to investigate how the fracture pattern of DI is changed under the effect of plastic deformation. For this reason, the prime objective of the current paper is to investigate the effect of plastic deformation on fracture property of DI after hot extrusion and after ambient temperature compression of the extruded samples. Additionally, the paper highlights some microstructural features of DI in its deformed state.

2. Materials and Experimental Methods

DI which chemical composition is listed in TABLE 1 was melted in a 150 kg induction furnace. Melt treatment involved spheroidising processing followed by inoculating one, which were carried out in a ladle using a commercial FeSi75Mg7Ca03 modifier and then foundry silicon of FeSi75 grade. The treated liquid metal was cast at 1310°C into bentonite moulds to produce cylindrical ingots of 60 mm in diameter and 300 mm in length.

[1] SLOVAK UNIVERSITY OF TECHNOLOGY, FACULTY OF MATERIALS SCIENCE AND TECHNOLOGY, J. BOTTU 25, TRNAVA, 917 24 SLOVAKIA
[2] NATIONAL ACADEMY OF SCIENCES OF BELARUS, PHYSICAL TECHNICAL INSTITUTE, 10. KUPREVICHA STR., MINSK, 220141 BELARUS

* Corresponding authors: alexander.chaus@stuba.sk

The ingots were cut into samples suitable for the hot extrusion and for the corresponding analyses and tests.

TABLE 1

Chemical composition of the used DI, wt. %

C	Si	Mn	Cr	Ni	Mg	P	S	Fe
3.52	1.98	0.61	0.14	0.35	0.042	0.068	0.011	Bal.

Cast samples were subjected to hot extrusion at 1000°C with varying plastic strain to be 20, 60 and 80% under the conditions schematically shown in Fig. 1. After extrusion, all hot-extruded samples had the same finale diameter (12.5 mm) however each initial diameter was varied to provide the corresponding strain value. Tensile tests were conducted on a ZD-15 universal testing machine (Germany) at room temperature and at an elongation rate of 0.5 mm/min using standard samples 6 mm in diameter and a gauge length of 30 mm as schematically presented in Fig. 2a. Two sets of cylindrical samples 5 mm in diameter and 9 mm in height, cut out from the extruded rods in the longitudinal and transverse cross-sections with respect to the direction of action of the deforming force during hot extrusion were subjected to compression according to the schemes shown in Fig. 2b and c. The compression tests were carried out on a ZD-15 universal testing machine (Germany) with a maximum compression force of 15 tons at ambient temperature. The compression rate was 5 mm per minute. In each experiment five samples were always used.

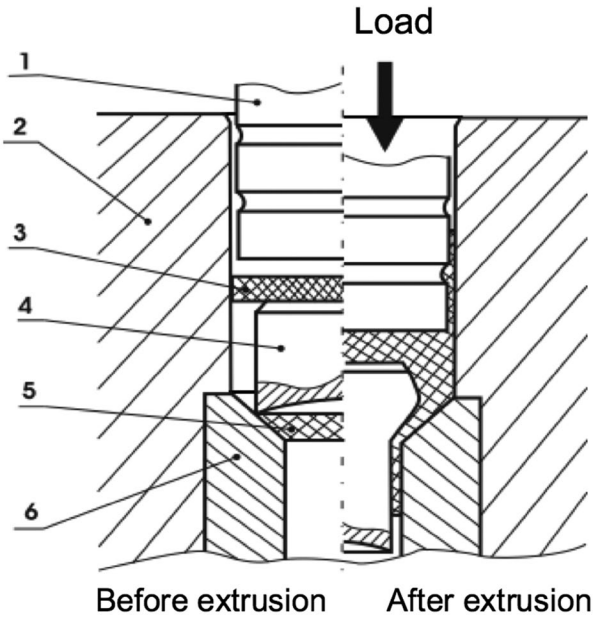

Fig. 1. Schematic diagram of the experimental arrangement for the hot extrusion of DI: 1 – Punch, 2 – Container, 3 – Graphite insert, 4 – Billet, 5 – Press remainder of graphite, 6 – Die

Metallographic samples were observed and analysed with a Neophot-32 light microscope (LM) and a JEOL JSM-7600F scanning electron microscope (SEM), and the fractured surfaces of the samples were examined using above-mentioned SEM. Samples were etched with 3% nital.

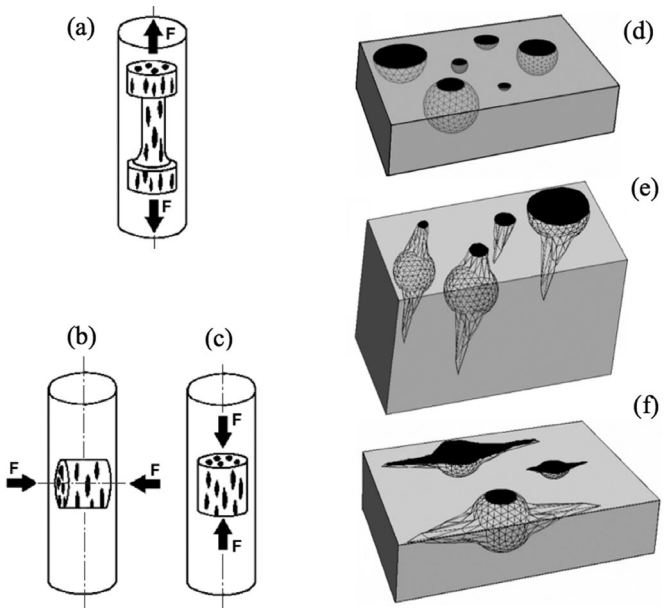

Fig. 2. Schemes of cutting out samples from extruded bars for (a) the tensile tests and (b, c) the compressive tests, and schematic representation of the shape of graphite spheroids randomly distributed in the (d) as-cast state and after hot extrusion in the (e) transverse and (f) longitudinal cross-sections relative to the direction of the principal plastic strain during extrusion: F – force

3. Results and Discussion

3.1. Microstructure and properties of DI subjected to hot extrusion

Schematic representation of the shape of graphite spheroids randomly distributed in the as-cast state and after hot extrusion in the transverse and longitudinal cross-sections relative to the direction of the principal plastic strain during extrusion is introduced in Fig. 2d, e and f respectively. SEM image in Fig. 3a shows the real 2D shape of graphite spheroids in the unetched as-cast microstructure while LM images in Fig. 3c and e illustrate the overall as-cast microstructure of DI iron in the etched samples where a mixed pearlitic-ferritic matrix can be clearly observed. It is seen that pearlite dominates the matrix and significantly smaller amount of ferrite surrounds practically each graphite spheroid. It is very important that perfect shape of graphite spheroids is proven by metallographic analysis that is in line with the scheme in Fig. 2d.

As follows from the scheme in Fig. 2e, graphite spheroids in the transverse cross-section of the extruded samples must remain their 2D shape unchanged independently on the plastic strain. Indeed, the metallographic examination shows that some plastic deformation of spheroids occurred in the transverse cross-section leading to the appearance of the deformed areas on their sides in the form of protrusions that in turn resulted in the violation of the perfect chape of spheroids. This was more evident in the case of the largest plastic strain that is illustrated in Fig. 3b, d and f.

Fig. 4 shows that plastic strain with the rate of 60 and 80% resulted in substantial overall changes of the microstructure in

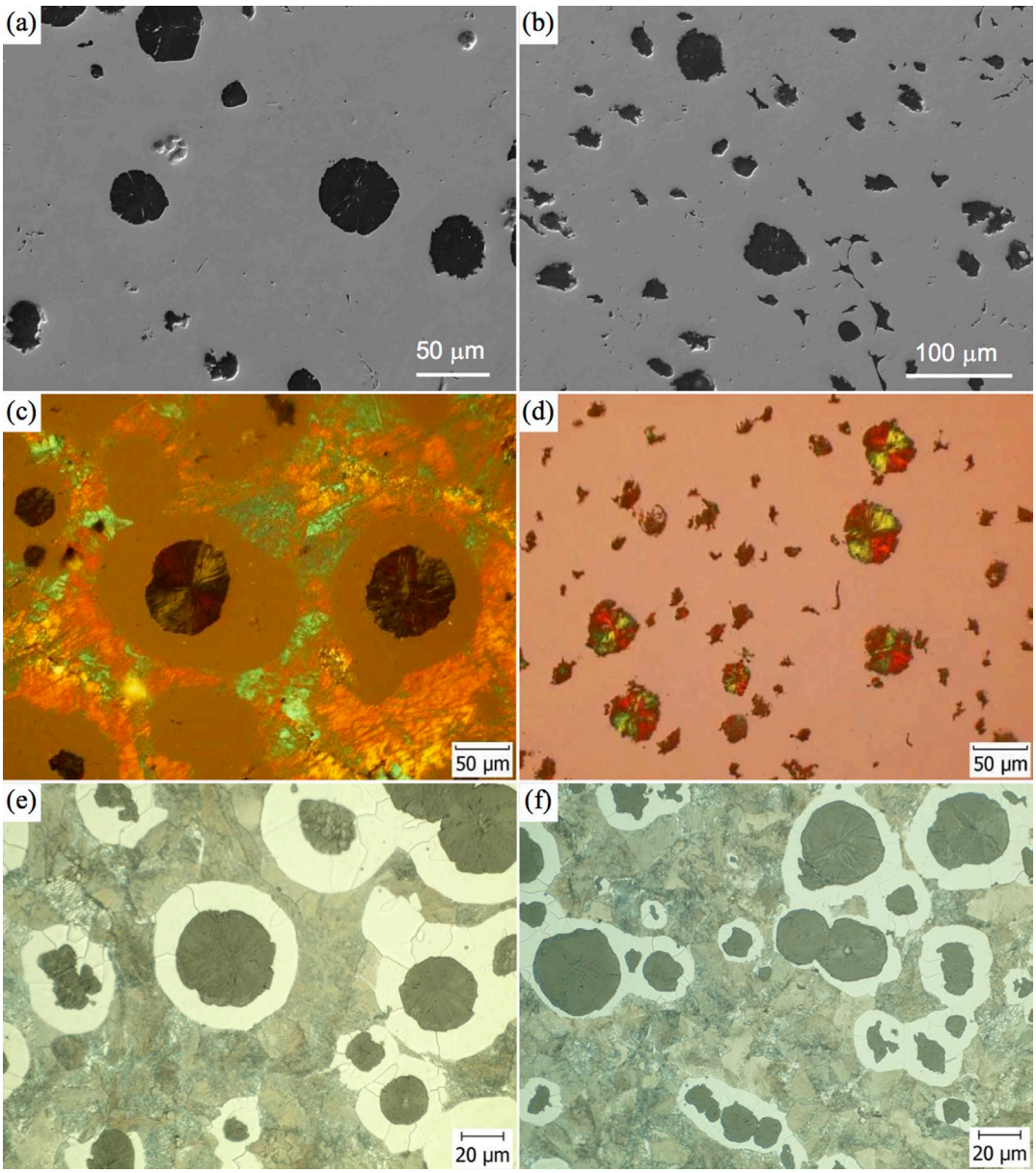

Fig. 3. Microstructure of DI after (a, c, e) casting and after (b, d, f) hot extrusion with plastic strain of 80%, in transverse cross-section: (a) and (b) Unetched samples, (c) and (d) in polarised light, (e) and (f) etched samples. (a) Adapted from [18]

the longitudinal cross-sections of the extruded samples. Primarily graphite spheroids tended to change their shape from initial spheroidal to oval-like, when strain was 20%, and then to moderate spindle (at ε = 60%), Fig. 4a, c and e, and very slim spindle (ε = 80%), Fig. 4b, d and f. In this context it should be stressed that similar changes in the sense of graphite shape evidently varying in transverse and longitudinal directions were observed in ferritic DI after high plastic strain levels during compression tests at room temperature [26] and at high temperatures [27-29]. It should be emphasised that in the latter work the matrix type was not introduced, however both the ferritic and mostly pearlitic matrixes could be observed in the studied samples. The change of graphite shape in DI under the effect of hot rolling in the longitudinal rolling direction has been also reported [30,31]. All these papers have shown that graphite spheroids are deformed and elongated mostly in the direction of plastic strain that is accompanied by a gradual transition from spheroidal to spindle shape of graphite particles, and the latter depends on a plastic strain applied. In this context, it is worth noting that the structural changes in the DI under the effect of dynamic deformation was also investigated however to the lesser extent [32,33].

On the other hand, a plastic flow of the metal matrix occurred during extrusion as can be seen in Fig. 4e and f for longitudinal direction of the plastic strain. It is very important that in the hot deformed DI a strong refinement of the matrix with respect to both the pearlite and ferrite constituents was proven, which is well seen when compared both images in Fig. 5. The microstructure refinement can be attributed to dynamic recrystallisation of the matrix occurred during hot extrusion. In this context it should be stressed that the same findings in the sense of the occurrence of dynamic recrystallisation under hot deformation of DI were reported in [28]. No doubt, that the

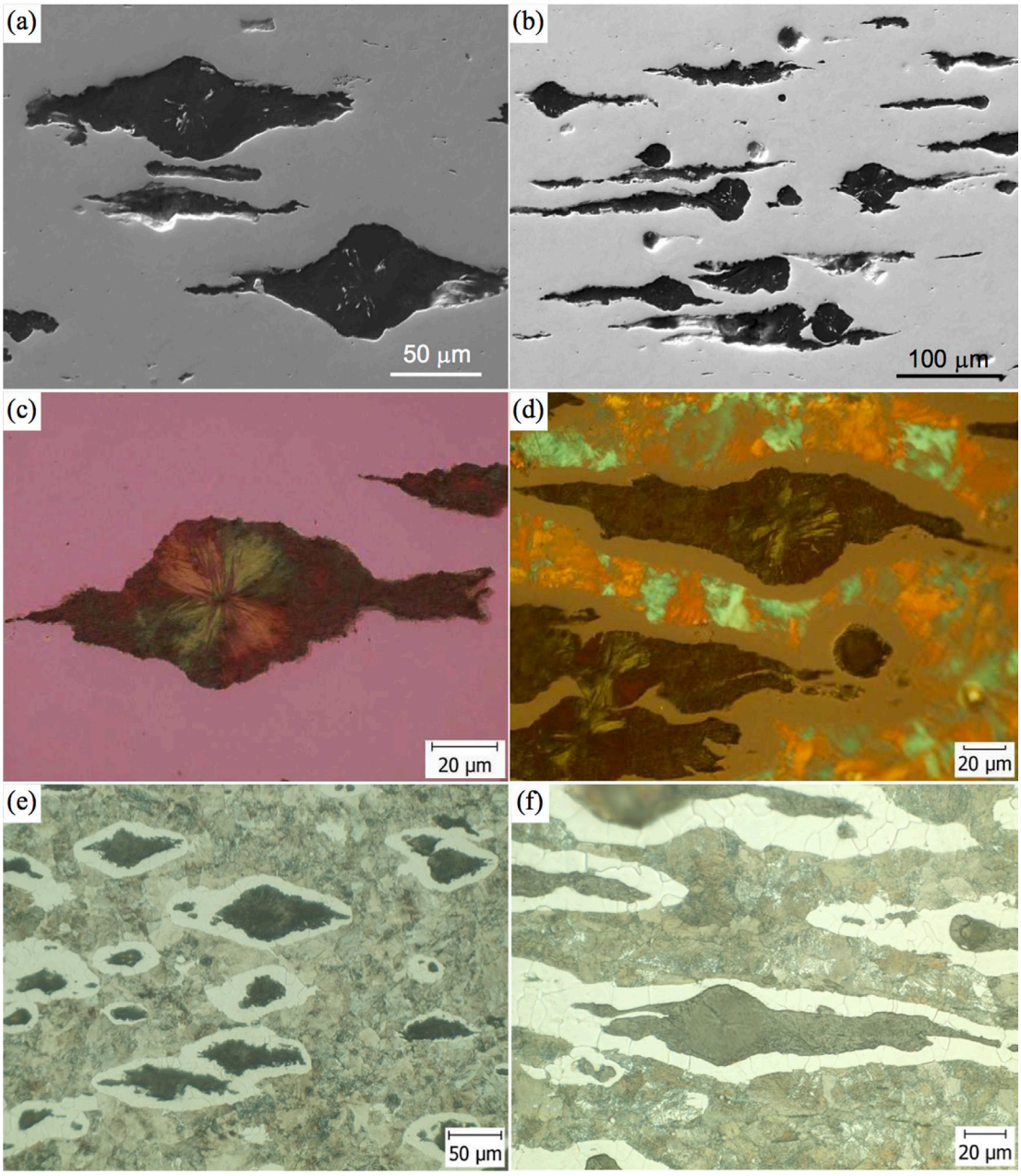

Fig. 4. Microstructure of DI after hot extrusion with plastic strain of (a, c, e) 60 and (b, d, f) 80%, in longitudinal cross-section: (a) and (b) Un-etched samples, (c) and (d) in polarised light, (e) and (f) etched samples

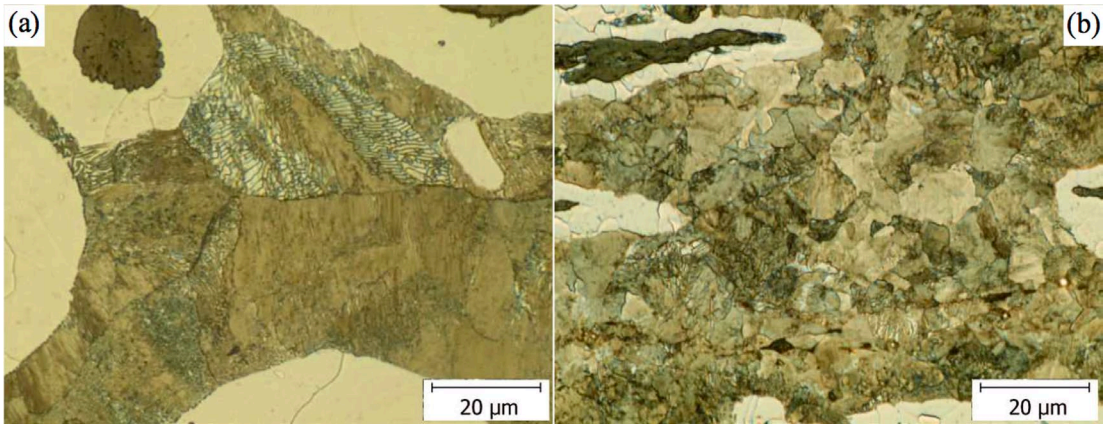

Fig. 5. Effect of the hot extrusion on the matrix refinement. Microstructure of DI after (a) casting and after (b) hot extrusion with plastic strain of 80%, etched samples

gradual increase in the ultimate tensile strength of DI subjected to the hot extrusion, as presented in Fig. 6, can be referred to the progressively enhanced microstructure refinement (primarily of pearlite) with increasing strain.

The results of the fracture analysis of the as-cast and extruded samples subjected to the tensile tests according to the scheme in Fig. 2a are in line with the above-mentioned findings. Fig. 7a shows overall fracture surface of the as-cast sample where the failure mode of the matrix appeared to be mainly brittle transgranular. Fig. 7b shows that with respect to graphite spheroids fracture preferentially occurred by a debonding mechanism at the graphite spheroid/matrix interface leading to the exposure of the very spheroids or voids in the places of their extraction at the fracture surface. In this context, it should be pointed out that such matrix-graphite spheroid debonding mechanism was not observed in the case of ferritic DI [34].

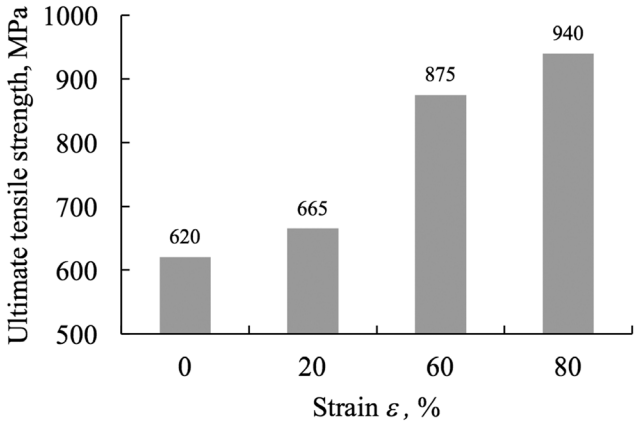

Fig. 6. Effect of the hot extrusion on the ultimate tensile strength of DI. Adapted from [24]

In contrast to the as-cast sample, in the extruded samples so-called quasi-cleavage facets are observed on the fracture surfaces, which varying size and depth reflect increasing plasticity and fracture energy values before damage due to a higher microstructure refinement of the matrix with increasing plastic strain, Fig. 7c, e and g. In the context of the plasticity and fracture energy values it should be stressed that all these observations are only supported by the failure analysis because actual stress-strain curves or elongation data were not obtained in the original work [24] from which the values of the tensile strength were adopted. It is worth mentioning that in this case graphite spindles failed in their cross-sections, i.e., their transgranular fracture occurred, that is well seen at higher magnification in Fig. 7d, f and h. The most important finding is that no cracks are observed in the microstructure after the extrusion and on the fracture surfaces after the tensile tests as confirmed in Figs. 3 and 4 and Fig. 7 respectively. In general, it is worthy of note that fatigue fracture of DI has been thoroughly examined [7,22,35-37]. On the other hand, a smaller number of investigations on fracture of conventional DI after tensile tests can be found in the literature [3,5,34] and any information is absent concerning fracture of hot extruded DI.

3.2. Microstructure and properties of hot extruded DI after compression tests

Main features of the microstructure of the extruded DI at the fracture surface after sample failure during ambient compression according to the sample loading schemes presented in Fig. 2b and c are shown in Fig. 8a, c and e and 8b, d, f, and g respectively. A cursory glance at the images in Fig. 8 reveals significantly severer plastic flow of DI under the influence of shear strain during the compression in both directions, according to Fig. 2b and c, compared with that under the hot extrusion, see Fig. 3b, d, and f and Fig. 4. As a consequence, significantly deformed and even broken graphite particles in the sense of their initial spherical shape are observed in the microstructure of the compressed samples previously hot-extruded with a higher strain, i.e., 80 %, see Fig. 8e and f. These features are more distinguished for the samples compressed according to the scheme in Fig. 2c rather than in Fig. 2b. Another feature is the appearance of the secondary cracks near the fracture surface that is illustrated, for example, in Fig. 8a and g.

Moreover, in the case of the sample previously deformed with a higher strain (80%) and compressed in the longitudinal direction (Fig. 9a), shear stresses led to the rotation of graphite spindles in certain depth along the fracture surface, which was observed on both sides of the crack propagation and schematically and metallographically illustrated in Fig. 9b and c, d respectively. As can be seen on the top circular base of the damaged cylindrical sample the location of the damaging shear stresses was at a depth of about one mm (restricted by red dashed lines) as presented in Fig. 9c. Comparing the starting and final location and orientation of spindles in the longitudinal cross-section in a central part of the cylindrical sample at the distance of several μm from the crack (left area on the image in Fig. 9d) and near this crack (right area on the image in Fig. 9d) respectively, it is seen that the graphite spindles turned during the compression at an angle of 90°. This is due to strong plastic flow of the extruded DI along the crack.

The plastic strain dependence of the compressive strength of a series of the previously hot extruded samples further compressed according to the schemes in Fig. 2b and c is shown in Fig. 10. The results of the compression tests show that compared with the as-cast state, a marked improvement in the compressive strength was achieved in all the studied samples. In general, the compressive strength shows a trend which is practically similar to the ultimate tensile strength as the strain is varied, i.e., the larger previous plastic strain in the extruded sample, the higher compressive strength. This general trend can be also explained by the microstructure refinement due to dynamic recrystallisation in the extruded samples (see Fig. 5). However, there was one exception which was not in line with the general trend; the sample extruded with a largest strain, i.e., 80%, and compressed in a direction normal to the extrusion direction, exhibited a lower value of compressive strength than the similarly compressed sample extruded with a lower strain, 60%. The simple explanation is that some threshold of stresses should exist above which brittle damage of elongated graphite spindles occurred due to

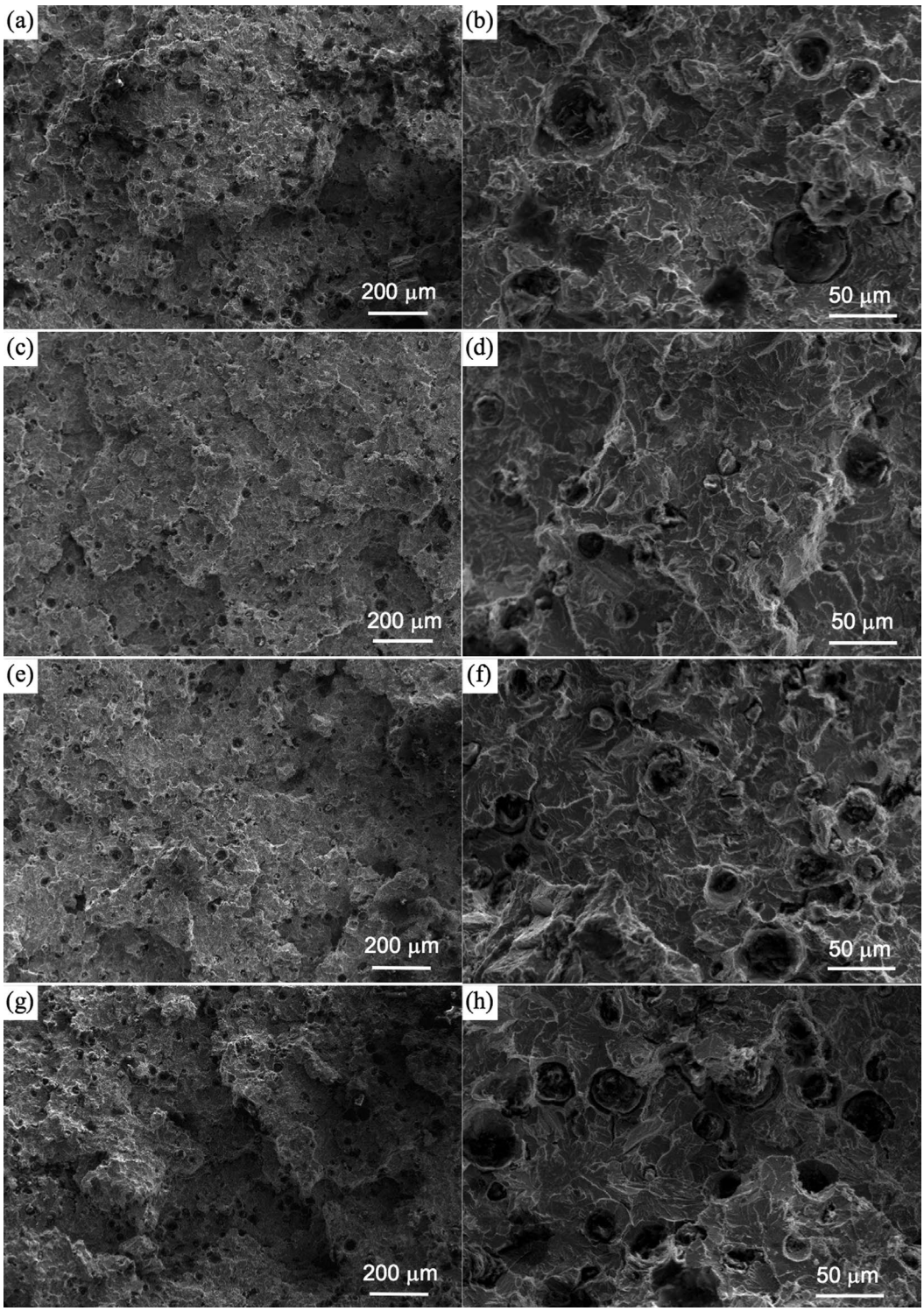

Fig. 7. Fracture surfaces of DI after the tensile tests: (a, b) as-cast samples and hot extruded samples with plastic strain of (c, d) 20%, (e, f) 60% and (g, h) 80%

plastic flow. This in turn could result in the deterioration of the matrix strength despite the microstructure refinement which is well seen in Fig. 8e and f. It is in this context important to realise that the resistance of elongated graphite spindles to the plastic strain should depend on their orientation against the first direction of applied compressive load. It is well known that the fracture occurred easier in the case when elongated particles are situated perpendicularly to the direction of a compressive load.

It is worth mentioning that some microstructural features illustrated in Fig. 8 are reflected in the development of fracture surfaces in the corresponding samples as presented in Fig. 11. Primarily the smearing of fracture surfaces, formed by cleavage mechanism, through strong plastic deformation is evidently seen in all the samples reflecting enhanced plastic flow of DI under the influence of large shear stresses. Fig. 11 also shows that the plastic flow of the material at the fracture surface caused the for-

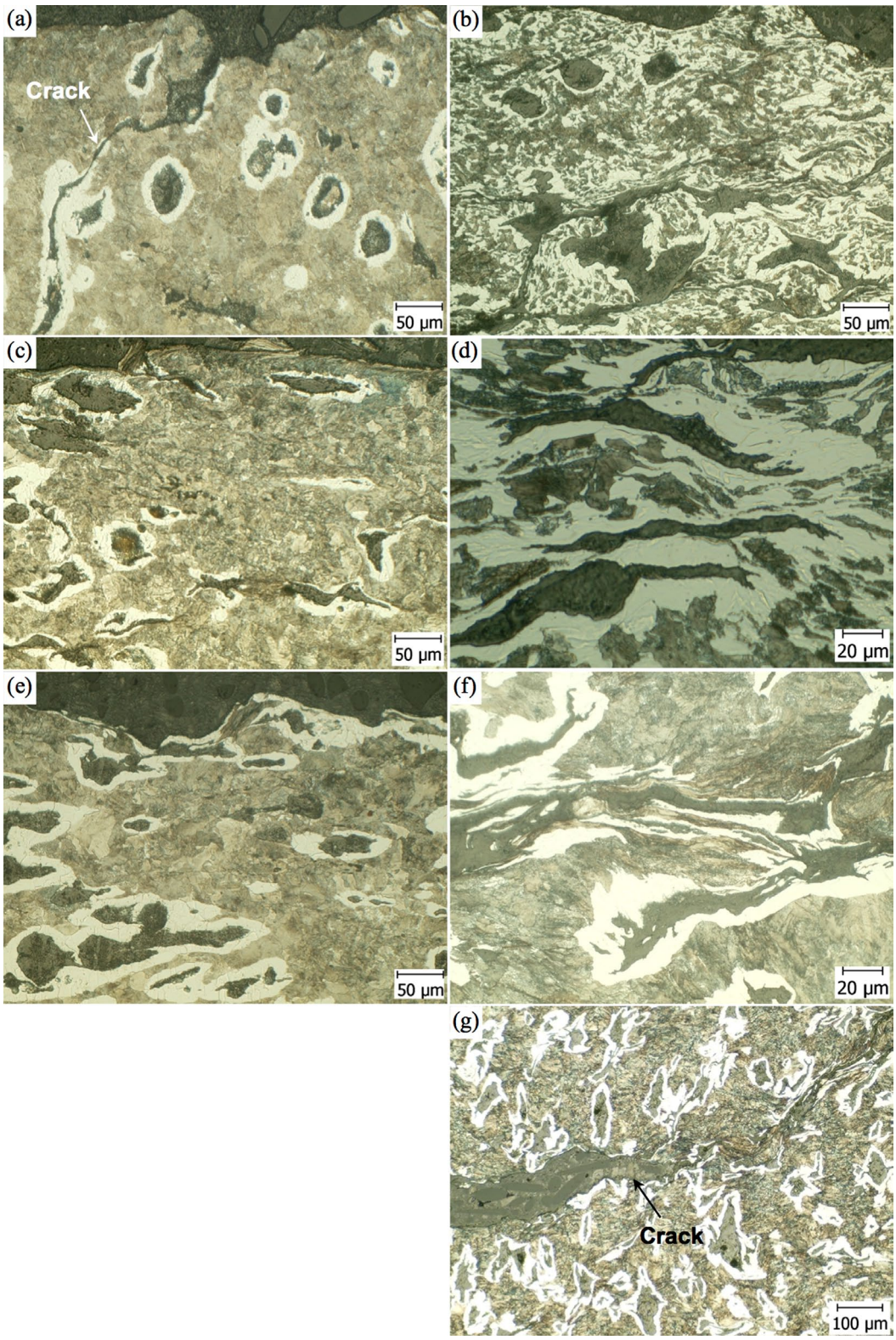

Fig. 8. Microstructure of the extruded DI samples at the fracture surfaces after failure during compression tests conducted according to the sample loading scheme in (a, c, e) Fig. 2b and (b, d, f, g) Fig. 2c. Plastic strain after the hot extrusion was (a, b) 20%, (c, d) 60% and (e, f, g) 80%, etched samples

mation of so-called "microscopic tongues" on the fracture surfaces. Moreover, in the case of the as-cast sample, on its fracture surface the formation of voids at the interface between the matrix and graphite spheroids in the direction of plastic flow was found (see Fig. 11a), possibly due to different plasticity of the matrix and graphite spheroids. The presence of secondary microcracks on the fracture surface was also confirmed, see Fig. 11a and e. Finally, the fracture surfaces reflect the certain morphology of graphite particles to be typical for the corresponding samples as can be seen when compared Fig. 11 with Fig. 8.

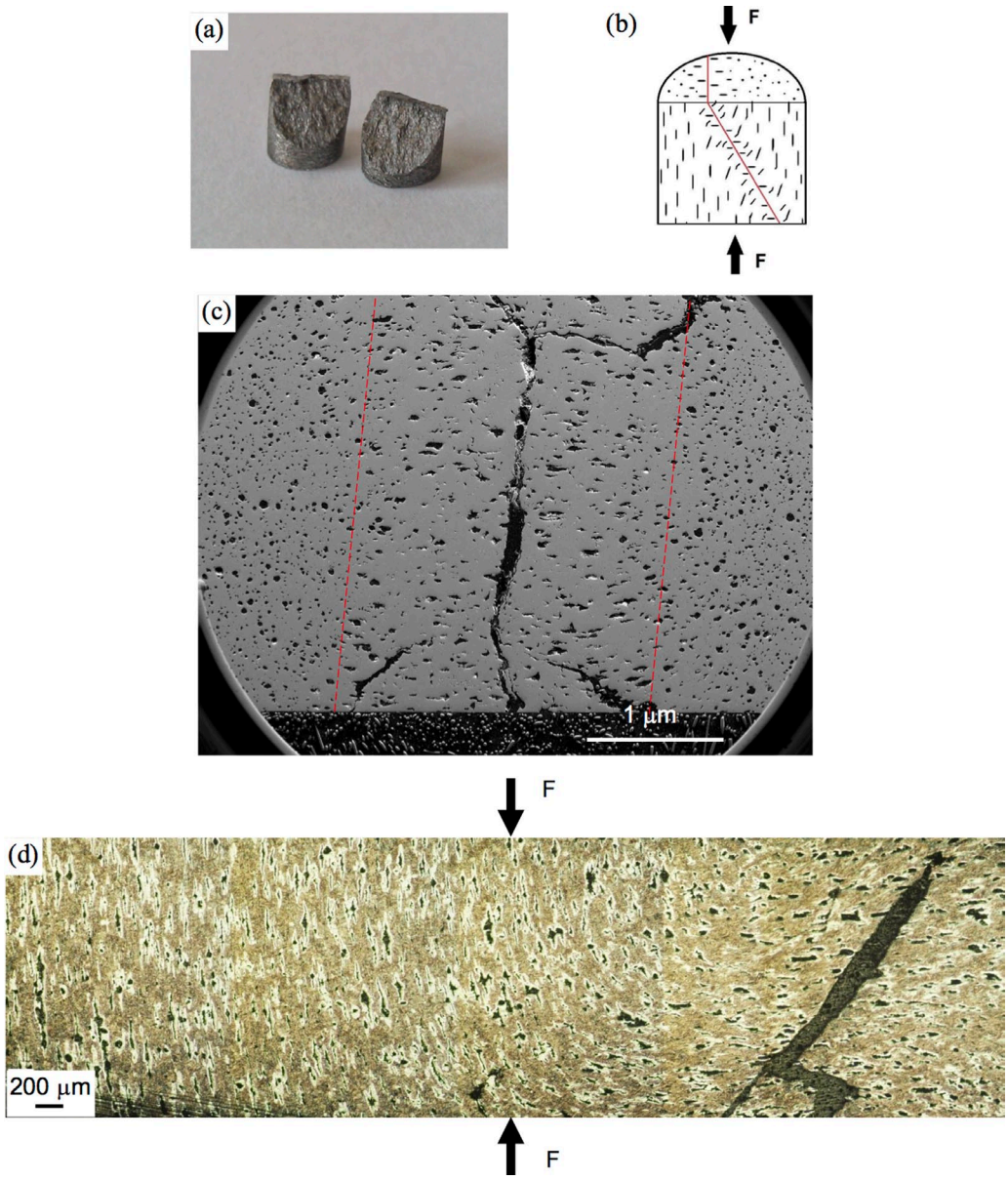

Fig. 9. (a, c, d) Metallographic and (b) schematic illustration of the microstructure transformation of the extruded DI (ε = 80%) occurred due to its strong plastic flow under the effect of shear stresses during compression and resulting in the rotation of graphite spindles in certain depth along the fracture surface: F – force, (c) unetched sample, (d) etched sample. Photomontage of LM images showing transformation of the microstructure in Fig. 9d is adapted from [38]

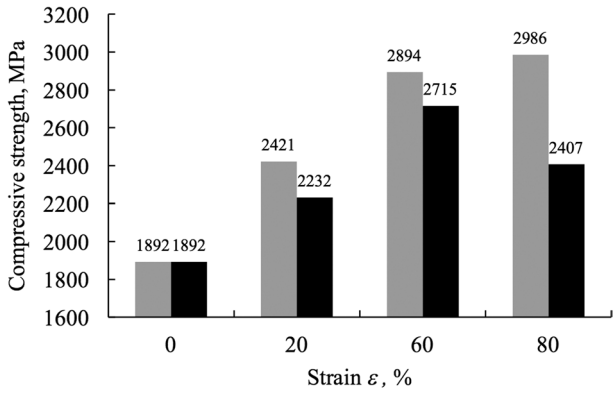

Fig. 10. Effect of the initial plastic strain due to extrusion on the compressive strength of DI: Gray and black bars reflect the compressive strength of the samples loaded during compression according to the scheme in Fig. 2c and b respectively. Adapted from [25]

4. Conclusions

The microstructure, properties, and fracture surfaces of pearlitic-ferritic DI in its as-cast state and after hot extrusion at 1000°C and after ambient compression of the extruded samples were investigated, and the following conclusions can be drawn:

1. The plastic strain during hot extrusion resulted in substantial changes of the initial as-cast microstructure with respect to the shape of graphite spheroids and the matrix refinement, which was more distinguish in longitudinal cross-sections of the extruded samples compared with that in the transverse cross-sections. With increasing strain graphite spheroids changed their shape to oval-like, then to moderate spindle, and finally to very slim spindle, and in the matrix progressively enhanced refinement of the pearlitic and ferritic

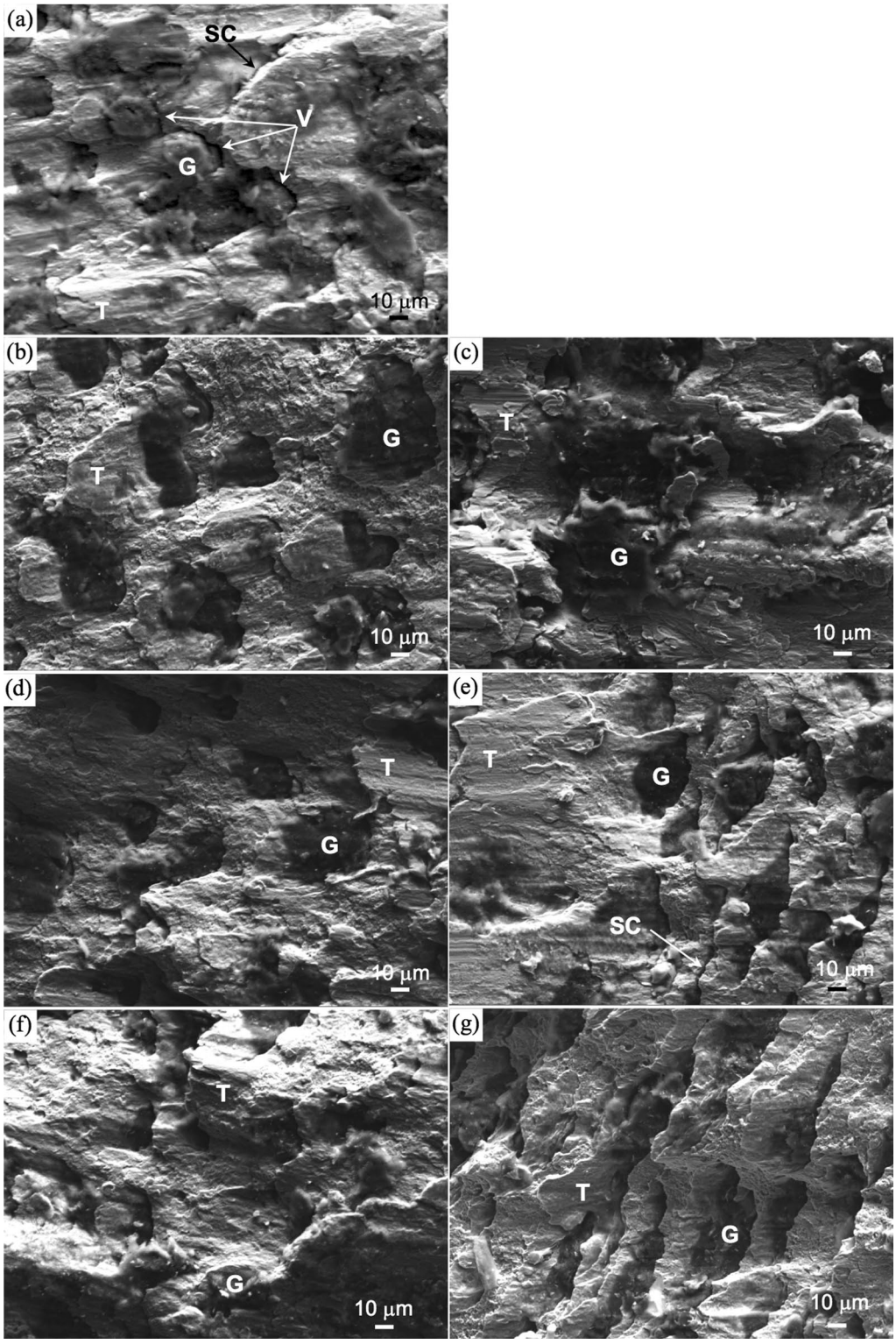

Fig. 11. Fracture surfaces of DI after the compressive tests of (a) as-cast sample and hot extruded samples with plastic strain of (b, c) 20%, (d, e) 60% and (f, g) 80%: SC – secondary crack, V – voids, G – graphite, T – microscopic tongues. During compression tests samples were loaded according to the scheme in (b, d, f) Fig. 2b and (c, e, g) Fig. 2c

constituents was occurred. The latter could be attributed to the dynamic recrystallisation of the pearlite and ferrite grains during hot extrusion, which was confirmed metallographically.

2. The above-mentioned refinement of the matrix, primarily in relation to pearlite, led to an increase in the ultimate tensile strength of the deformed DI. The investigation of fracture surfaces of samples subjected to the tensile tests revealed that in the as-cast samples fracture preferentially occurred by a debonding mechanism at the graphite spheroid/matrix interface, while in the case of the extruded samples graphite spindles failed in their cross-sections, i.e., by transgranular

mechanism. In general, varying size and depth of quasi-cleavage facets were consistent with the corresponding values of the tensile strength.

3. The metallographic examinations revealed lager microstructural changes due to severer plastic flow of DI under the influence of shear strain during the compression in both directions, i.e., parallel or perpendicular against the extrusion direction compared with the case of the hot extrusion. As a consequence, significantly deformed and even broken graphite particles were observed in the microstructure of the compressed samples. These features are more distinguished for the samples compressed in the longitudinal direction. The secondary cracks near the fracture surface were revealed in the microstructure of the compressed samples that was not the case after extrusion. In the sample previously deformed with a higher strain (80%) and compressed in the longitudinal direction, shear stresses led to the rotation of graphite spindles in certain depth along the fracture surface.
4. Some microstructural features due to compression are reflected in the development of fracture surfaces in the compressed samples. Primarily the smearing of fracture surfaces, formed by cleavage mechanism, through strong plastic deformation was evidently seen in all the samples reflecting enhanced plastic flow of DI under the influence of large shear stresses. It is important that the hot extrusion enhanced the compressive strength of DI.

Acknowledgments

The financial support of the grants from the Ministry of Education, Science, Research and Sport of the Slovak Republic VEGA 1/0747/19 and VEGA 1/0796/20 is gratefully acknowledged. The authors are grateful to Dr Jaroslav Sojka for technical help and helpful discussions with respect to the results obtained in this work.

REFERENCES

[1] J.A. Pero-Sanz Elorz, D. Fernández González, L.F. Verdeja, Physical Metallurgy of Cast Irons, Springer (2018).
[2] F.D. Gelin, A.S. Chaus, Metallic Materials (In Russian), second ed., Vyshejshaya Shkola, Minsk (2007).
[3] G. Artola, A. Monzón J. Lacaze, J. Sertucha, Mater. Sci. Eng. A **831**, 142206 (2022).
[4] A. Mussa, P. Krakhmalev, J. Bergstrom, Wear **498-499**, 204305 (2022).
[5] C. Liu, Y. Du, T. Ying, L. Zhang, X. Zhang, X. Wang, G. Yan, B. Jiang, Mater. Today Commun. **31**, 103522 (2022).
[6] T. Wigger, T. Andriollo, C. Xu, S.J. Clark, Z. Gong, R.C. Atwood, J.H. Hattel, N.S. Tiedje, P.D. Lee, M.A. Azeem, Acta Mater. **221**, 117367 (2021).
[7] M. Benedetti, V. Fontanari, D. Lusuardi, Eng. Fract. Mech. **206**, 427-441 (2019).
[8] J. Qing, S. Lekakh, M. Xu, D. Field, Carbon **171**, 276-288 (2021).
[9] D.M. Stefanescu, G. Alonso, R. Suarez, Metals **10**, 221 (2020).
[10] I. Riposan, M. Chisamera, S. Stan, Mater. Sci. Forum **925** (3), 3-11 (2018).
[11] U. Tewary, D. Paul, H.K. Mehtani, S. Bhagavath, A. Alankar, G. Mohapatra, S.S. Sahay, A.S. Panwar, S. Karagadde, I. Samajdar, Acta Mater. **226**, 117660 (2022).
[12] D.M. Stefanescu, G. Alonso, P. Larrañaga, E. De la Fuente, R. Suarez, Acta Mater. **107**, 102-126 (2016).
[13] K. Theuwissen, J. Lacaze, L. Laffont, Carbon **96**, 1120-1128 (2016).
[14] D.D. Double, A. Hellawell, Acta Metall. Mater. **43**, 2435-2442 (1995).
[15] T. Skaland, O. Grong, T. Grong, Metall. Trans. A **24A**, 232-2345 (1993).
[16] W.C. Johnson, H.B. Smartt, Metall. Trans. A **8**, 553-565 (1977).
[17] A.S. Chaus, Met. Sci. Heat Treat. **57** (7-8), 419-427 (2015).
[18] A.S. Chaus, J. Soka, Ľ. Čaplovič, Met. Sci. Heat Treat. **55** (3-4), 175-180 (2013).
[19] Z.-Q. Shen, X.-L. Tian, H.-L. Zheng, T.-T. Li, Y. Xu, R.-F. Xu, N. Zhang, Foundry **61** (4), 357-361 (2012).
[20] J.K. Solberg, M.I. Onsøien, Mater. Sci. Technol. **17**, 1238-1242 (2001).
[21] T. Skaland, O. Grong, and T. A. Grong, Metall. Trans. A, **24**, 2321-2345 (1993).
[22] W. Zhou, D.O. Northwood, C. Liu, J. Mater. Res. Technol. **15** (12), 3836-3849 (2021).
[23] J. Bača, A.S. Chaus, Met. Sci. Heat Treat. **46** (5-6), 188-191 (2004).
[24] A.S. Chaus, J. Sojka, A.I. Pokrovskii, Phys. Met. Metallogr. **114** (1), 85-94 (2013).
[25] A.I. Pokrovskii, Hot Plastic Deformation of Cast Iron. Structure, Properties, Technological Fundamentals, Belaruskaya Navuka, Minsk, 2010 [in Russian].
[26] I. Hervas, M. Ben Bettaieb, A. Thuault, E. Hug, Mater. Des. **52**, 524-532 (2013).
[27] K. Qi, F. Yu, F. Bai, Z. Yan, Z. Wang, T. Li, Mater. Des. **30**, 4511-4515 (2009).
[28] X. Zhao, X. Yang, T. Jing, J. Iron. Steel Res. Int. **18**, 48-51 (2011).
[29] X. Zhao, T.F. Jing, Y.W. Gao, G.Y. Qiao, J.F. Zhou, W. Wang, J. Mater. Sci. **39**, 6093-6096 (2004).
[30] A. V. Lisovsky , B. A. Romantsev, Metallurgist **54**, 173-177 (2010).
[31] T. El Bitar , E. El Banna, Mater. Lett. **31**, 145-150 (1997).
[32] G. Iannitti, A. Ruggiero, N. Bonora, S. Masaggia, F. Veneri, Theor. Appl. Fract. Mech. **92**, 351-359 (2017).
[33] D. Myszka, L. Cybula, A. Wieczorek, Arch. Metall. Mater. **59** (3), 1171-1179 (2014).
[34] F. Iacoviello, O. Di Bartolomeo, V. Di Cocco, V. Piacente, Mater. Sci. Eng. A **478**, 181-186 (2008).
[35] T. Borsato, P. Ferro, A. Fabrizi, F. Berto, C. Carollo, Int. J. Fatigue **145**, 106137 (2021).
[36] S.N. Lekakh, M. Buchely, R. O'Malley, L. Godlewski, Mei Li, Int. J. Fatigue **148**, 106218 (2021).
[37] P. Čanžar, Z. Tonkovic, J. Kodvanj, Mater. Sci. Eng. A **556**, 88-99 (2012).
[38] A.S. Chaus, Phys. Met. Metallogr. **115** (7), 672-681 (2014).